

Supplemental Material

Chaos in Hamiltonian systems subjected to parameter drift

Dániel Jánosi, Tamás Tél

S1 Snapshot elliptic points

We linearize (2) around $x = \pm 1$ by writing $x = \pm 1 + \delta$ and keeping only linear terms in δ to get

$$\ddot{\delta} = -2\delta + (\varepsilon + \alpha t) \cos \omega t, \quad t \geq 0. \quad (\text{S1})$$

This equation is valid for motions remaining in a small vicinity of $x = 1$ or $x = -1$ all the time. Its homogeneous part describes a harmonic oscillation with eigenfrequency of modulus $\omega_0 = \sqrt{2}$, whose general solution is $c_+ e^{\lambda_+ t} + c_- e^{\lambda_- t}$ with $\lambda_{\pm} = \pm i\sqrt{2}$. By looking for the particular solution in the form

$$\delta_p = A \cos \omega t + B \sin \omega t + Ct \cos \omega t,$$

the coefficients turn out to be $A = \varepsilon/(2 - \omega^2)$, $B = 2\alpha\omega/(2 - \omega^2)^2$, and $C = \alpha/(2 - \omega^2)$. Note that the vanishing of the denominators at $\omega = \sqrt{2}$ hints on a resonance which occurs when $\omega = \omega_0 = \sqrt{2}$. The general solution is thus

$$\delta(t) = c_+ e^{\lambda_+ t} + c_- e^{\lambda_- t} + \frac{\varepsilon}{2 - \omega^2} \cos \omega t + 2 \frac{\alpha\omega}{(2 - \omega^2)^2} \sin \omega t + \frac{\alpha}{2 - \omega^2} t \cos \omega t, \quad (\text{S2})$$

and the velocity is $v(t) = \dot{\delta}(t)$. With initial conditions $\delta(0)$, $v(0)$ coefficients c_{\pm} become determined and take the form

$$c_+ = \frac{i\sqrt{2}(\delta(0) - \delta_{E,0}^*) + (v(0) - v_{E,0}^*)}{i2\sqrt{2}}, \quad c_- = \frac{i\sqrt{2}(\delta(0) - \delta_{E,0}^*) - (v(0) - v_{E,0}^*)}{i2\sqrt{2}}, \quad (\text{S3})$$

with $\delta_{E,0}^* = \varepsilon/(2 - \omega^2)$, $v_{E,0}^* = \alpha(2 + \omega^2)/(2 - \omega^2)^2$. By bringing the particular solution on the left hand side, the general solution can be written as

$$\delta(t) - \delta^*(t) = c_1 e^{\lambda_+ t} + c_2 e^{\lambda_- t}. \quad (\text{S4})$$

The quantity

$$\delta^*(t) = \delta_p(t) = \frac{\varepsilon + \alpha t}{2 - \omega^2} \cos \omega t + 2 \frac{\alpha\omega}{(2 - \omega^2)^2} \sin \omega t \quad (\text{S5})$$

should be considered as the instantaneous position (relative to ± 1) of a *time-dependent elliptic point*. Its velocity coordinate is

$$v^*(t) = \dot{\delta}^*(t) = -\frac{(\varepsilon + \alpha t)\omega}{2 - \omega^2} \sin \omega t + \alpha \frac{2 + \omega^2}{(2 - \omega^2)^2} \cos \omega t. \quad (\text{S6})$$

We thus see that the shifts appearing in the parantheses of the coefficients c_{\pm} are just the initial position and velocity of the elliptic points. It is remarkable that the frequency about the moving elliptic point remains $\omega_0 = \sqrt{2}$ at any time, the same as the eigenfrequency of the undriven ($\varepsilon = \alpha = 0$) problem. Expressions (S5), (S6) can therefore be considered to define a *snapshot elliptic point*, SEP:

$$\delta_E^*(t) = \delta^*(t), \quad v_E^*(t) = v^*(t).$$

On the stroboscopic map $\delta_E^*(t = nT) = \delta_{E,n}^*$ and $v_E^*(t = nT) = v_{E,n}^*$. The expressions in (3) and (4) of the main text are the phase space coordinates of the SEPs determined here taken with $\omega = 1$.

The gray curve in Fig.S1 represents the trajectory of the SEP about $x = 1$ in continuous time. The stroboscopic locations are marked with orange dots. Numerically obtained snapshot tori belonging to a few time instances appear as continuous curves of different color. The analytically determined SEP is indeed in their middle at any instant. These are small tori on the scale of the whole phase space, they do not deform too much over such a short time interval. Their translation is, however, clearly visible with a slight amplitude increase.

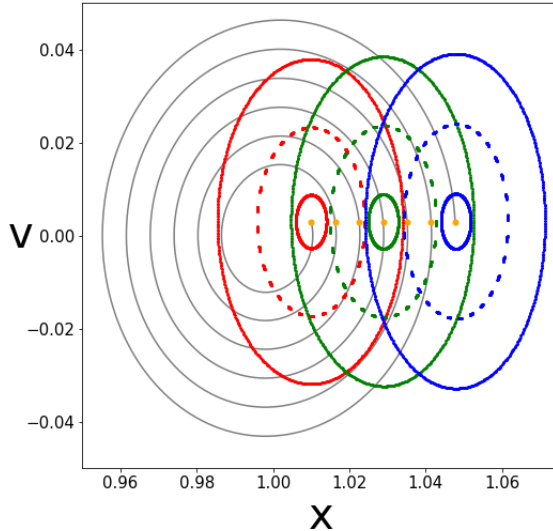


Figure S1: Snapshot elliptic points and snapshot tori in the phase space. The analytically obtained continuous time coordinates of (3) valid about $x = 1$ is shown in gray, the stroboscopic locations given by (4) are the orange dots for $n = 0, \dots, 6$ ($\varepsilon = 0.01, \alpha = 0.001$). The red curves mark initial tori belonging to $t = n = 0$, while green and blue curves represent their images taken with dynamics (2) plotted in green (blue) after $n=3$ (6) iterations.

Let us consider now the motion of the SEPs in a combined scenario consisting of an increasing and a decreasing ramp making a full return to the original driving amplitude possible. In more detail, this scenario, applied also in Section S6, is characterized by a driving amplitude $\varepsilon + \alpha t$ during the first n periods, but the amplitude changes to $\varepsilon + nT - \alpha(t - nT) = \varepsilon - \alpha(t - 2nT)$ in the interval $nT \leq t \leq 2nT$, i.e. during an additional n of periods. On the increasing ramp, for $0 \leq t < nT$, (S5) remains valid leading to the SEP position

$$\delta_{E,n}^* = \frac{\varepsilon + \alpha nT}{2 - \omega^2}, \quad v_{E,n}^* = \alpha \frac{2 + \omega^2}{(2 - \omega^2)^2} \quad (\text{S7})$$

by the end of the n th period. Relations (S5), (S6) suggest that for $t \geq nT$ the time dependence of the SEP is

$$\delta^*(t) = \frac{\varepsilon - \alpha(t - 2nT)}{2 - \omega^2} \cos(\omega(t - nT)) - 2 \frac{\alpha\omega}{(2 - \omega^2)^2} \sin(\omega(t - nT)), \quad (\text{S8})$$

$$v^*(t) = -\frac{\varepsilon - \alpha(t - 2nT)}{2 - \omega^2} \omega \sin(\omega(t - nT)) - \alpha \frac{2 + \omega^2}{(2 - \omega^2)^2} \cos(\omega(t - nT)). \quad (\text{S9})$$

This solution would, however, yield the SEP coordinates

$$\tilde{\delta}^* = \frac{\varepsilon + \alpha nT}{2 - \omega^2}, \quad \tilde{v}^* = -\alpha \frac{2 + \omega^2}{(2 - \omega^2)^2}$$

by time nT , different from (S7) in the velocity coordinate. The SEP is expected to be at any time a solution of the differential equation (2), and should therefore be a continuous and differentiable function of time. A way to find such a solution is based on realizing that a trivial rearrangement of (S4) was

$$\delta(t) - \delta^*(t) = c_+ e^{\lambda+t} + c_- e^{\lambda-t} - C_+ e^{\lambda+t} - C_- e^{\lambda-t} = c'_+ e^{\lambda+t} + c'_- e^{\lambda-t} \quad (\text{S10})$$

with arbitrary C_+, C_- shows that the elliptic nature of the moving point remains but the original position $\delta^*(t)$ becomes shifted by $C_+ e^{\lambda+t} + C_- e^{\lambda-t}$. Since $\lambda_{\pm} = \pm i\sqrt{2}$, these terms can also be represented as $D \sin \sqrt{2}t + E \cos \sqrt{2}t$ with some real D and E . We can therefore assume that the time-dependent location of the SEP is, for $t \geq nT$,

$$\delta^*(t) = \frac{\varepsilon - \alpha(t - 2nT)}{2 - \omega^2} \cos \omega t - 2 \frac{\alpha \omega}{(2 - \omega^2)^2} \sin \omega t + D \sin [\sqrt{2}(t - nT)] + E \cos [\sqrt{2}(t - nT)], \quad (\text{S11})$$

$$v^*(t) = -\frac{\varepsilon - \alpha(t - 2nT)}{2 - \omega^2} \omega \sin \omega t - \alpha \frac{2 + \omega^2}{(2 - \omega^2)^2} \cos \omega t + D\sqrt{2} \cos [\sqrt{2}(t - nT)] - E\sqrt{2} \sin [\sqrt{2}(t - nT)],$$

where in the argument of the trigonometric functions we have used that $\omega nT = 2\pi n$. The coefficients can be fixed by prescribing continuity, by requiring the values of $\delta^*(t = nT)$ and $v^*(t = nT)$ to match those of (S7). This leads to $\delta_{E,n}^* = \tilde{\delta}^* + E$, $v_{E,n}^* = \tilde{v}^* + \sqrt{2}D$, which yields

$$D = \alpha\sqrt{2} \frac{2 + \omega^2}{(2 - \omega^2)^2}, \quad E = 0.$$

By substituting these into (S11), we obtain the position coordinate $\delta^*(t)$ of the SEP valid for $nT \leq t \leq 2nT$. The coordinates of the SEP at time $t = 2nT$ are then found to be

$$\delta_{E,2n}^* = \frac{\varepsilon}{2 - \omega^2} + \alpha\sqrt{2} \frac{2 + \omega^2}{(2 - \omega^2)^2} \sin \sqrt{2}nT = \delta_{E,0}^* + \alpha\sqrt{2} \frac{2 + \omega^2}{(2 - \omega^2)^2} \sin \sqrt{2}nT, \quad (\text{S12})$$

$$v_{E,2n}^* = -\alpha \frac{2 + \omega^2}{(2 - \omega^2)^2} + \alpha \frac{2 + \omega^2}{(2 - \omega^2)^2} 2 \cos \sqrt{2}nT = v_{E,0}^* - 2\alpha \frac{2 + \omega^2}{(2 - \omega^2)^2} (1 - \cos \sqrt{2}nT). \quad (\text{S13})$$

The SEP coordinates are thus different from their initial values $\delta_{E,0}^*, v_{E,0}^*$ at the end of the scenario in spite of the return of the driving amplitude to its original value. This hysteresis disappears only in the limit $\alpha \rightarrow 0$, i.e. quasistatically slow scenarios.

With nonzero α rate, both the continuous time SEP trajectories and their stroboscopic locations are qualitatively different on the decreasing ramp from those of the increasing one. Fig.S2 shows this for an $n = 4$ step process. The continuous trajectory on the decreasing ramp (red curve) is much less spiral-like, than the increasing counterpart. The sequence of stroboscopic points appears to be much more irregular here than with positive α (as treated in Fig.S1), however, can be described with the simple formulas (S12) and (S13).

The SEPs with phase space coordinates $(\pm 1 + \delta_{E,2n}^*, v_{E,2n}^*)$ are plotted as orange dots in panel (c) of Fig.S7 for $\omega = 1$, $T = 2\pi$, where a hysteresis of the full snapshot phase space can also be seen.

S2 A snapshot hyperbolic point

Assuming that the motion remains all the time close to the origin, from the linearization of (2) we obtain

$$\ddot{x} = x + (\varepsilon + \alpha t) \cos \omega t, \quad t \geq 0. \quad (\text{S14})$$

The homogeneous part of this equation describes an exponential instability with eigenvalues $\lambda_{\pm} = \pm 1$, and its general solution is $c_+ e^t + c_- e^{-t}$. By looking for the particular solution in the form

$$x_p = A \cos \omega t + B \sin \omega t + Ct \cos \omega t,$$

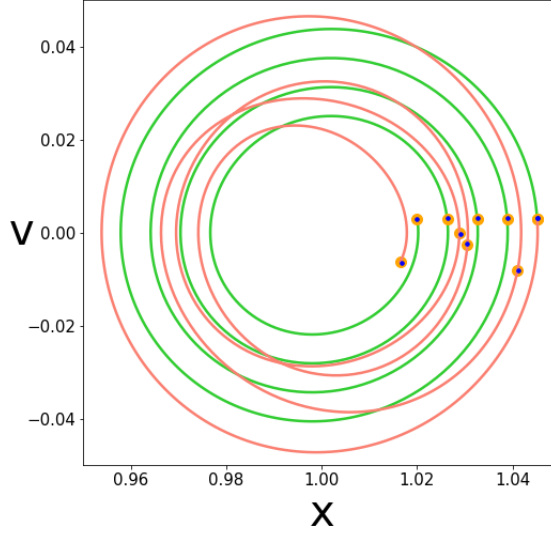


Figure S2: Motion of the SEP about $x = 1$ in a scenario with full return to the original driving amplitude $\varepsilon = 0.02$ ($\omega = 1$). Green curve: trajectory of the SEP on the increasing ramp of length $n = 4$ for $\alpha = 0.001$ in continuous time. Red curve: trajectory of the SEP on the decreasing ramp for $\alpha = -0.001$ in continuous time. Orange dots: analytic stroboscopic locations according to (4) on the increasing ramp, and according to (S12) and (S13) on the decreasing one. Blue dots: numerically obtained SEP positions initiated from $x_{E,0}^*, v_{E,0}^*$, and evolved under (2). We can see that the numerical result follows the analytical one quite well.

the coefficients turn out to be $A = -\varepsilon/(1 + \omega^2)$, $B = 2\alpha\omega^2/(1 + \omega^2)^2$, and $C = -\alpha/(1 + \omega^2)$. The general solution is thus

$$x(t) = c_+ e^t + c_- e^{-t} - \frac{\varepsilon}{1 + \omega^2} \cos \omega t + 2 \frac{\alpha\omega}{(1 + \omega^2)^2} \sin \omega t - \frac{\alpha}{1 + \omega^2} t \cos \omega t, \quad (\text{S15})$$

and the velocity is $v(t) = \dot{x}(t)$. With initial conditions $x(0)$, $v(0)$ coefficients c_{\pm} become determined and take the form

$$c_+ = \frac{x(0) - x_{H,0}^* + (v(0) - v_{H,0}^*)}{2}, \quad c_- = \frac{x(0) - x_{H,0}^* - (v(0) - v_{H,0}^*)}{2}, \quad (\text{S16})$$

with $x_{H,0}^* = -\varepsilon/(1 + \omega^2)$, $v_{H,0}^* = \alpha(\omega^2 - 1)/(1 + \omega^2)^2$. By bringing the particular solution on the left hand side, the general solution can be written as

$$x(t) - x^*(t) = c_+ e^t + c_- e^{-t}. \quad (\text{S17})$$

The quantity

$$x^*(t) = x_p(t) = -\frac{\varepsilon + \alpha t}{1 + \omega^2} \cos \omega t + 2 \frac{\alpha\omega}{(1 + \omega^2)^2} \sin \omega t \quad (\text{S18})$$

should be considered as the instantaneous position of a *time-dependent hyperbolic point*. Its velocity coordinate is

$$v^*(t) = \dot{x}_p(t) = \frac{(\varepsilon + \alpha t)\omega}{1 + \omega^2} \sin \omega t + \alpha \frac{\omega^2 - 1}{(1 + \omega^2)^2} \cos \omega t. \quad (\text{S19})$$

We see again that the shifts appearing in the parantheses of coefficients c_{\pm} are just the initial position of the hyperbolic point and its velocity. It is remarkable that the eigenvalues about the time-dependent hyperbolic point remain $\lambda_{\pm} = \pm 1$ at *any time*, the same as the stability exponents of the undriven ($\varepsilon = \alpha = 0$) problem. Moreover, this also holds true for the *eigenvectors*. The one belonging to $\lambda_+ = 1$ is $(1, 1)$, the local unstable

direction is thus the main diagonal, the other one is $(1, -1)$ the local stable direction is the sub diagonal. Expressions (S18), (S19) can therefore be considered to define a *snapshot hyperbolic point*, SHP:

$$x_H^*(t) = x^*(t), \quad v_H^*(t) = v^*(t).$$

On the stroboscopic map $x_H^*(t = nT) = x_{H,n}^*$ and $v_H^*(t = nT) = v_{H,n}^*$. The expressions in (5) and (6) of the main text are the phase space coordinates of the SHPs determined here taken with $\omega = 1$.

S3 Break-up of an outermost KAM torus

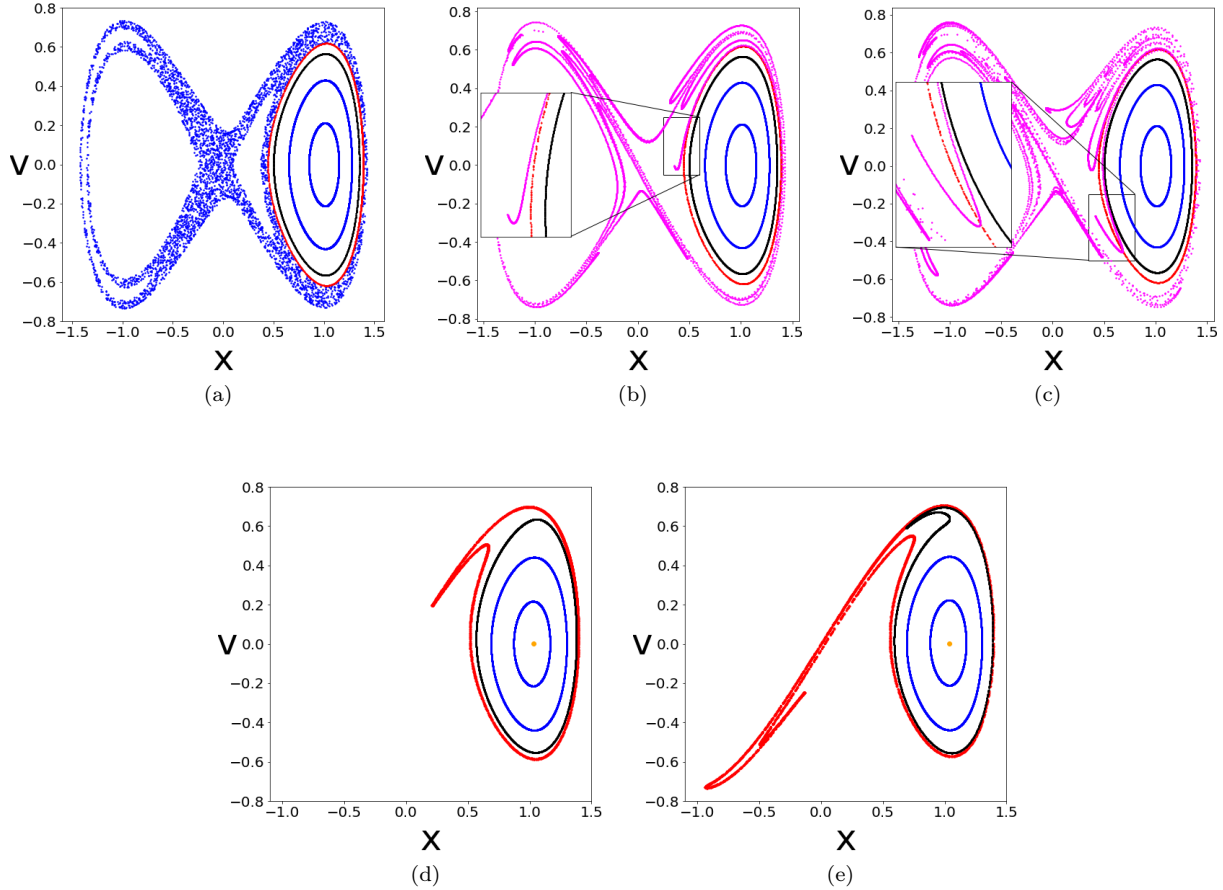


Figure S3: (a) Tori of system (1) generated from initial condition $x = 0.444236$ (red), $x = 0.5$ (black), $0.65, 0.85$ (blue), $v = 0$ ($\omega = 1$). Blue dots represent a chaotic sea (generated from the initial condition $x = 0.4, v = 0$) and is shown to be tangent to the outermost red torus. The red torus of Fig.6 is marked here with a black line. (b) The stable manifold of $x_{H,3}^*$ initiated from a segment of length $dl = 0.1$ plotted at time zero (pink curve), along with the set of the initial tori shown in panel (a). The inset shows that the pink and red curves have no common points yet. (c) The $dl = 0.1$ stable manifold of $x_{H,4}^*$ plotted at time zero (pink curve), along with the set of the initial tori of panel (a). The inset shows that the pink and red curves intersect (but the pink and black ones do not), i.e. indicating that $n_c = 4$ for the outermost torus. (d), (e) Shape of the set of tori of panel (a) after $n = 3$ and $n = 4$ iterates. In panel (e) the red torus comes close to the origin, proving that $n_c = 4$. The applied scenario is: $\varepsilon = 0.01$, $\alpha = 0.001$. In panels (d) and (e) orange dots mark snapshot elliptic points of the appropriate time instances given by (4).

S4 The PRA field compared with initial tori

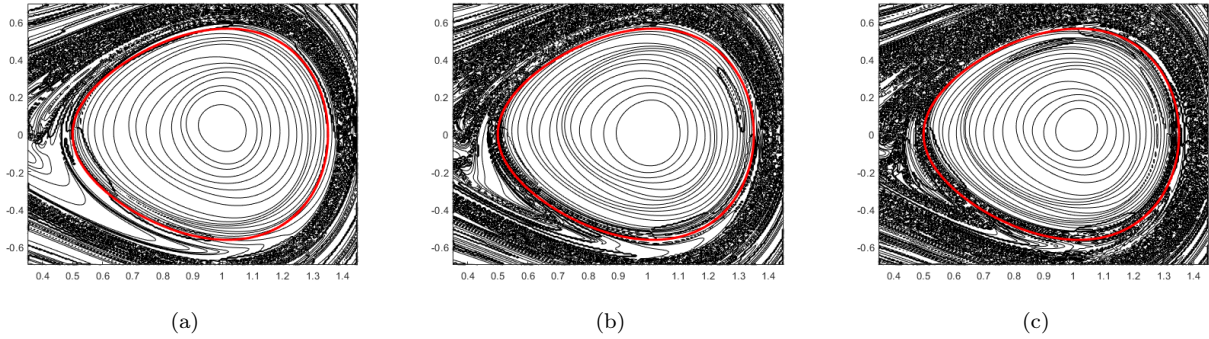


Figure S4: Level curves of the PRA field for periods $n = 4$ (a), $n = n_c = 5$ (b), and $n = 6$ (c) overlaid by the red initial torus of Fig.6. Dark regions mark irregular level lines of the PRA field. In panel (a) the red torus lies among smooth level lines. It enters part of the dark region by $n = n_c$, and this is more enhanced by $n = 6$.

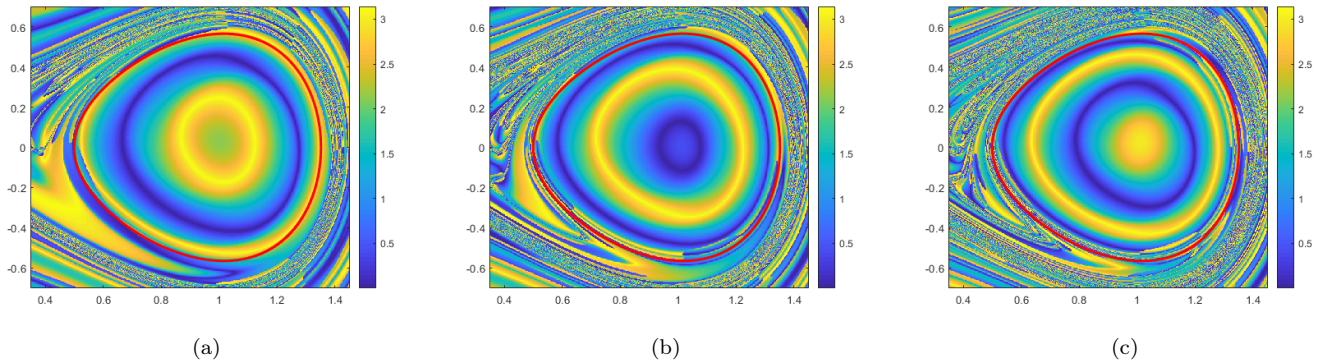


Figure S5: Colormap of the PRA field and the red torus with the same parameters than those of Fig.S4. Here, irregular regions are indicated by the mixing of colors. As seen before, the red torus enters this irregular region on panel (b), where $n = n_c = 5$. The colorbars indicate the PRA value.

S5 Scenarios with decreasing driving amplitudes

In scenarios taken with negative α rates torus break-up might take place, just like in scenarios with positive rates. This is illustrated by Fig.S6 where we see part of the initial phase space belonging to $\varepsilon = 0.04$, the end stage of the scenario at $\varepsilon \approx -0.0856$, and the stationary case belonging to this driving amplitude. Panel (b) illustrates the strong deformation of snapshot tori. This is the break-up instant for the yellow torus, while the red one broke up 2 iterates earlier. The extension of the chaotic sea in this last stage is larger than in the initial state (a) due to the break-up of large outer tori (e.g. the yellow one) surrounding the stationary chaotic sea at $\varepsilon = 0.04$. In the stationary phase portrait belonging to the final value of the driving amplitude, $\varepsilon \approx -0.0856$ (c), the chaotic sea is also larger than in panel (a), clearly indicated by the red and yellow trajectories being parts of the chaotic sea in this case. This phenomenon can be attributed to the driving amplitude changing its sign during the scenario. In some other cases the size of the chaotic region in the end state turns out to be larger than in the stationary case belonging to this driving amplitude, but in our system, in these cases tori do not break up.

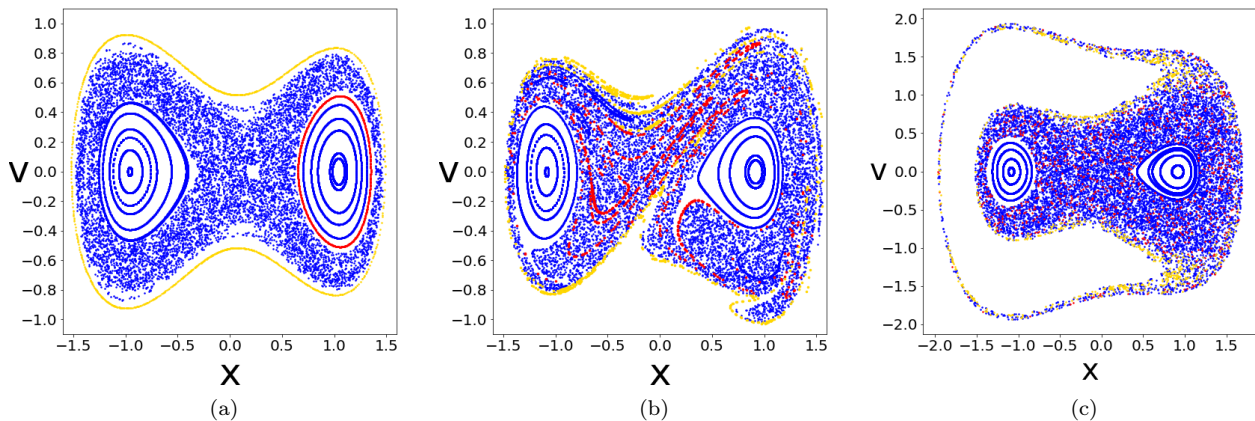


Figure S6: Snapshot phase portrait in a scenario with decreasing amplitude $\alpha = -0.001$ ($\omega = 1$). (a) The initial phase space with stationary $\varepsilon = 0.04$ generated from 21 symmetrical initial conditions between $x = -1.4, \dots, 1.4$ (blue points), $x = 1.35$ (red torus) and $x = -1.52$ (yellow torus), while $v = 0$. (b) End state of the scenario $\varepsilon = 0.04$ $\alpha = -0.001$ after $n = 20$ iterates at final driving amplitude $\varepsilon \approx -0.0856$. (c) Stationary case belonging to $\varepsilon \approx -0.0856$ visualized with the same set of initial conditions as in panel (a), where we can see that the initial conditions for the red and yellow trajectories are now inside the chaotic sea.

S6 Scenarios with full return of the driving amplitude

In scenarios containing an increasing and a decreasing ramp with the same magnitude of α leading to a full return of the driving amplitude, a hysteresis takes place. The end state deviates from the initial state due to the nonzero rate of change of the amplitude, and because the snapshot tori at the end of the increasing ramp are not tori of the stationary case belonging to that driving amplitude. An illustrative example is given in Fig.S7, where an increase of the extension of the chaotic sea can again be seen. Part of the inward extension is due to the break-up of all tori existing originally in the white region between the blue band and the red tori.

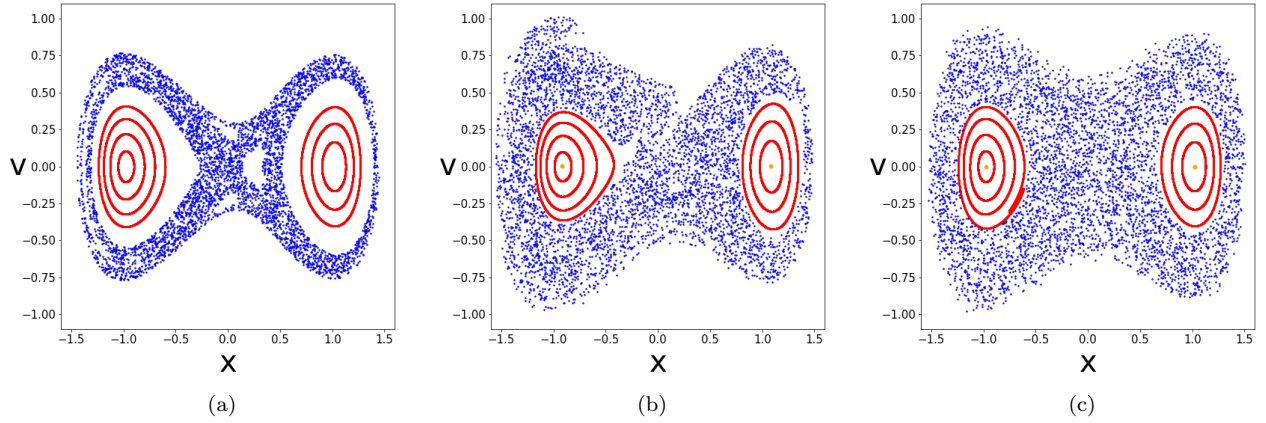


Figure S7: Snapshot phase portraits in a scenario with full return of the driving amplitude ($\omega = 1$). (a) The initial phase space with stationary $\varepsilon = 0.02$ generated from initial conditions $x = 0.7, 0.8, 0.9, -0.6, -0.7, -0.8, -0.9$ (red tori), 0.5 (blue dots representing a chaotic sea), while $v = 0$. (b) Mid state of the full scenario, i.e. the end state of scenario: $\varepsilon = 0.02$, $\alpha = 0.0005$ after $n = 20$ iterates at maximum driving amplitude $\varepsilon \approx 0.0828$. (c) End state after the decreasing part of the scenario taken with rate $-\alpha$, and starting with panel (b) as initial condition, after an additional $n = 20$ iterations back at the initial amplitude $\varepsilon = 0.02$. In panels (b) and (c) orange dots mark the snapshot elliptic points of (4) with $n = 20$, and of (S12), (S13) with $2n = 40$, respectively.